Journal of Applied Electrochemistry **29**: 577–584, 1999.

A statistical analysis of the electrodeposition of nickel in the presence of a magnetic field

J. C. SHANNON, Z. H. GU and T. Z. FAHIDY*
Department of Chemical Engineering, University of Waterloo, Waterloo, Ontario, Canada N2L 3G1
*(*author for correspondence)*

Received 8 December 1997; accepted in revised form 19 August 1998

Key words: CSLBM, FBM analysis, magnetic fields, nickel deposition

Abstract

Statistical analysis has been applied to study the effect of magnetic fields on the electrodeposition of nickel in terms of (i) fractional Brownian theory applied to its rate, and (ii) a variance-based analysis of the deposit surface roughness determined by confocal scanning laser beam microscopy.

1. Introduction

The production of smooth nickel deposits of uniform thickness and physical properties, in general, is an important technological goal. Pulsed plating is effective in improving significantly the crystal structure of electrolytic coating [1, 2] but at the expense of production efficiency. Pursuant to an earlier work on the effect of externally imposed magnetic fields on cathodic nickel deposition [3], the utilization of magnetic fields has received renewed attention [4–6]. Confocal scanning laser beam microscopy (CSLBM) [7] has been found convenient to study deposit structure and to supply necessary data for the examination of roughness distribution. Its application to copper etching [8], electrolytic copper refining [9], anodic passivation [10], anodic dissolution and cathodic deposition [11, 12] attest to the usefulness (although not to an exclusiveness) of this technique.

The purpose of this paper is twofold. First, experimentally observed variations of current under the influence of vertical and horizontal magnetic fields are examined in terms of fractional Brownian motion (FBM) theory to ascertain the degree of order in the cathodic process. These results are complemented by an in-depth statistical examination of surface roughness obtained via CSLBM. The results offer a quantitative measure of the magnetic field effect and indicate paths of its optimal utilization.

2. Experimental procedure

A 1 cm high, 4 cm inner diameter cylindrical Plexiglass cell was used for experiments. The cell contained a 1 cm wide, 1.5 cm inner diameter inlaid nickel anode ring centred at its top. The cathode was an 8 mm diameter inlaid copper disc centred at the bottom of the cell. Prior to each experiment, the cathode was first polished by 220 and 400 grade emery paper, then polished with 1 μm alumina to a mirror-like surface. The anode was also polished with 400 grade emery paper. An aqueous mixture of 1 mol dm^{-3} $NiCl_2.6H_2O$ containing 0.485 mol dm^{-3} boric acid and 0.220 mol dm^{-3} hydrogen peroxide served as electrolyte. Electrolysis was carried out via an HP Harrison 6203B regulated d.c. power supply, at cell voltage drops (CVD) increased in 0.05–0.1 V increments allowing the attainment of steady-state up to the operating CVD. Data logging was performed by a Fluke 45 multimeter interfaced with an IBM clone, at a sampling rate of 1 per s. The vertical magnetic field was produced by a Varian Model V-4005 d.c.-regulated electromagnet with a 4 in diameter pole face, and the horizontal magnetic field was produced by a Spectromagnetic Model 1019 d.c.-regulated 4 in variable gap electromagnet. The electrolytic cell was centered between the magnet pole faces, as shown in Figure 1.

Surface morphological examination of the cathodic nickel deposits was carried out by CSLBM applied to a 100×100 μm scanned area located as close to the

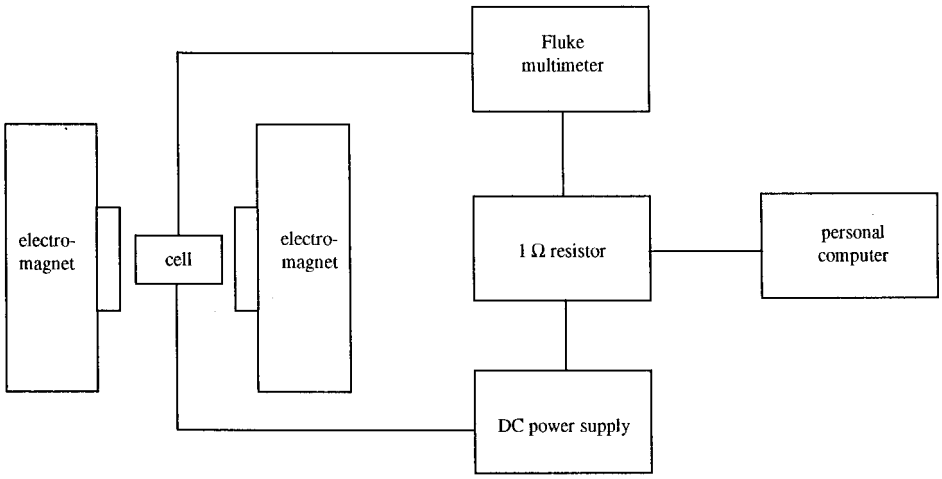

Fig. 1. Sketch of the experimental apparatus.

cathode centre as allowed by the apparatus. The depth profile images, digitized by MathCad 7 software were used to obtain line profiles, 3D images and surface roughness distribution. Microsoft Excel software was employed in the statistical analysis of the morphological information.

3. Results and analysis

3.1. *Time-series analysis of current variations with time*

Figure 2 illustrates typical experimental current–time variations observed at CVD = 1 V. The entire set of such observations was subjected to analysis via FBM theory [13] to determine pertinent numerical values of the Hurst exponent H from Pox diagrams. The application of Hurst analysis to electrochemical processes has been amply described in the recent literature (e.g. [14–16]) and is not repeated here. As shown in Table 1, H tends to decrease with an increase in CVD in both magnetic field configurations, hence the current/time variations exhibit an increasingly weaker structural correlation. The relatively low values of the coefficient of determination (r^2) at $H < 1/2$ offer a further indication of tendency towards chaotic behaviour.

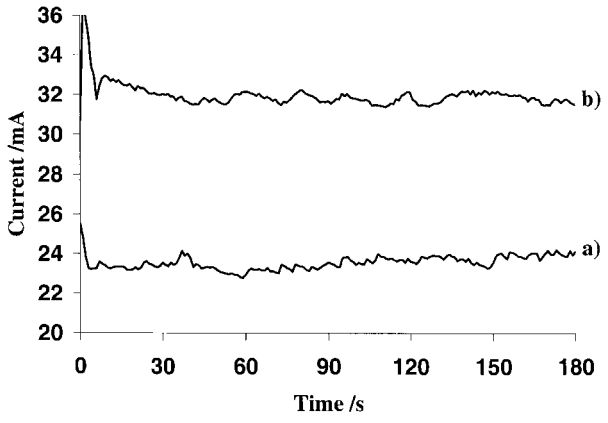

Fig. 2. A typical experimental current density–time observation at CVD = 1 V. (a) $B = 0$; (b) $B = 320$ mT vertical.

3.2. *Analysis of depth profiles and deposit roughness distribution*

Figure 3 is the micrograph of the cathode surface subjected to depth profile analysis. Figure 4 depicts a typical line profile, based on confocal images. Line

Table 1. Summary of the FBM-based analysis of the cathode current (Fig. 2)

B/mT	Direction	CVD/V	H	r^2
0	–	1.0	0.70	0.88
100	H	0.7	0.91	0.90
100	H	0.8	0.65	0.98
100	H	0.9	0.64	0.96
100	H	1.0	0.46	0.97
200	H	1.0	0.38	0.91
200	V	0.8	0.72	0.90
200	V	1.0	0.56	0.88
200	V	1.2	0.44	0.70
200	V	1.4	0.42	0.72
200	V	1.6	0.44	0.67

Legend
B: magnitude of the imposed magnetic flux density
Direction: H horizontal; V vertical
CVD: cell voltage drop
H: Hurst exponent, the slope of the Pox diagram
r^2: coefficient of determination related to the Pox diagram

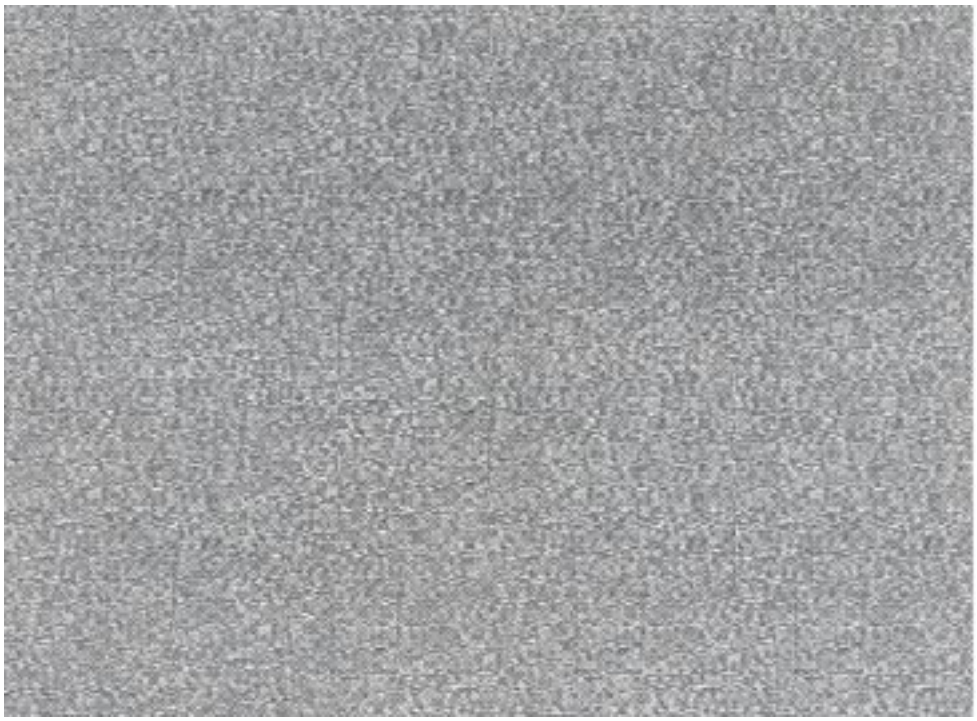

Fig. 3. A typical micrograph of an experimental cathodic nickel deposit at CVD = 1 V.

profiles were obtained in *x*- and *y*-directions, with the origin set at the upper left-hand apex of the image. The equidistant profiles were spaced at 20 μm intervals, that is, there were five profiles in each direction. Figure 5 shows the enlarged profile for the [40, 60 μm] subdistance. The sharp fluctuations in surface depth over a short distance might be an indirect indication of small grain size. Line profiles are especially useful for detecting variations in the local roughness against position, as indicated in Figure 6, where three consecutive lines within the same surface sample are shown at a total separation of 60 μm. The modified depth for each line is a linear shift in the measured line depth for the purpose of presentation.

The results of a variance-based analysis are summarised in Table 2. The entries represent depth values measured over the entire 512×512 (i.e., a total of 262 144 data points per experiment) pixel positions of the imaged cathode surface. The standard deviation (or the variance) of depths is a measure of the roughness

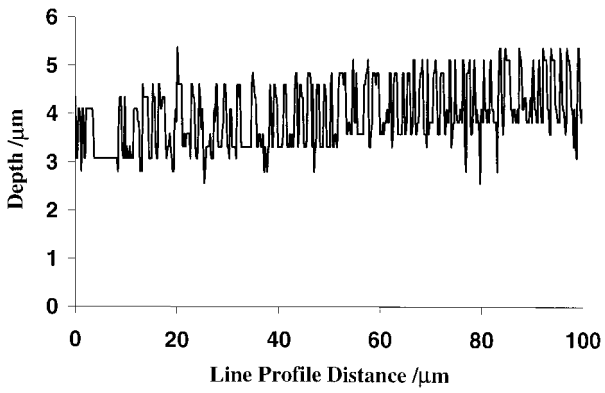

Fig. 4. Surface roughness distribution along a 100 μm horizontal line segment through the middle of the scanned surface area in a vertical magnetic field of flux density $B = 260$ mT, at CVD = 1 V.

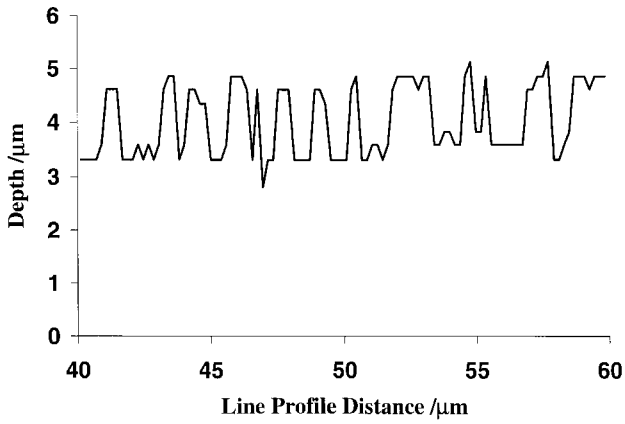

Fig. 5. Surface roughness distribution along the [40, 60 μm] section of the horizontal line segment in Figure 4.

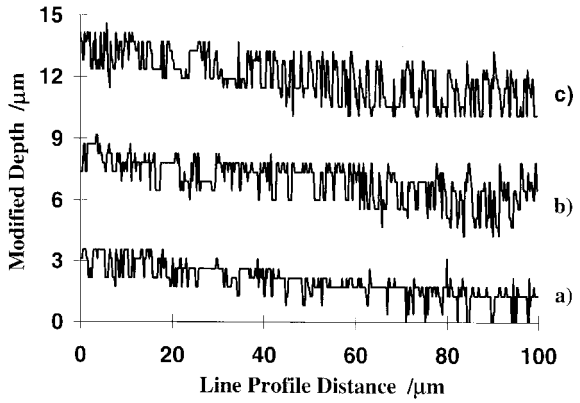

Fig. 6. A typical variation in morphology at $B = 90$ mT vertical, due to position within a sample, measured from the bottom of the 100×100 μm test area at distances of (a) 25, (b) 50 and (c) 75 μm. The line profiles have been shifted along the depth axis to separate them for viewing.

of the surface. The imposition of a magnetic field reduces, in general, surface roughness with respect to the absence of a magnetic field, but Figure 7 demonstrates the importance of field orientation. While the vertical field effect is by and large monotonic, the horizontal field effect is initially oscillatory ($B < 200$ mT), and the beneficial effect on surface quality is less pronounced than in the case of vertical fields.

For a better understanding of the behaviour of the standard deviation of surface depth, a twofold analysis was further performed on the cathode deposits (referred to in the sequel as samples). In the first set each surface was partitioned into 16 equal segments and analysed as described in the preceding paragraph. In the second set ten line profiles were selected for analysis by taking equally spaced lines at 0, 25, 50, 75 and 100 μm in the x- and y-direction. Data pertaining to the sections and the lines were used to test the homogeneity of depth variances via Bartlett's method, discussed briefly in the Appendix, as follows:

(i) The variance about the depth means was calculated and Bartlett's test was performed on the set of variances obtained (one variance per sample). This test indicates if there is a significant difference in depth gradients between samples, that is, if all samples have statistically equal location-dependent depth differences, or if the imposition of a magnetic field changes the depth gradients within the sample.

(ii) Within each sample, the variance within the lines or sections was tested via Bartlett's method. The test indicates the positional dependence of variance within a sample, that is, whether position influences roughness

Table 2. Summary of the overall sample statistics (CVD = IV) for depth profile

	H100	H200	H300	H400	V90	V260	V320	NMF
Mean	3.047	7.147	4.795	8.537	2.713	3.724	6.687	6.313
Std. dev.	0.775	1.623	1.388	1.295	1.347	0.781	0.883	1.973
Variance	0.601	2.633	1.926	1.677	1.813	0.610	0.694	3.891
Skewness	–0.569	0.030	–0.565	–0.345	–0.190	0.447	–0.639	–0.294
Kurtosis	–0.279	–0.524	0.721	–0.172	–0.647	0.896	0.641	–0.638
Max	6.800	11.793	8.959	12.484	9.872	7.186	9.292	11.459
Min	0.100	0.850	0.243	1.395	0.109	0.242	2.297	0.409
Ave. dev.	0.646	1.335	1.080	10.28	1.105	0.632	0.651	1.643
Conf(0.05)	0.003	0.006	0.005	0.005	0.005	0.003	0.003	0.008
Conf(0.01)	0.003	0.008	0.007	0.007	0.007	0.004	0.004	0.010
Median	3.241	6.959	4.720	8.592	2.681	3.593	6.484	6.413
Mode	3.241	6.959	5.154	8.592	3.128	3.593	6.484	7.778

Legend:
HX: horizontal magnetic field with X mT magnetic flux density
VX: vertical magnetic field with X mT magnetic flux density
NMF: no magnetic field
Mean: mean value of depth (μm)
Std. dev.: standard deviation of depth about the mean (μm)
Variance: variance deviation of depth about the mean (μm^2)
Max: largest value of depth (μm)
Min: lowest value of depth μm
Conf(0.05): confidence interval with $\alpha = 0.05$
Conf(0.01): confidence interval with $\alpha = 0.01$
Ave. dev: average magnitude of deviations from the mean value (μm)
Median: median value of depth (μm)
Mode: most frequency occuring value of depth (μm)

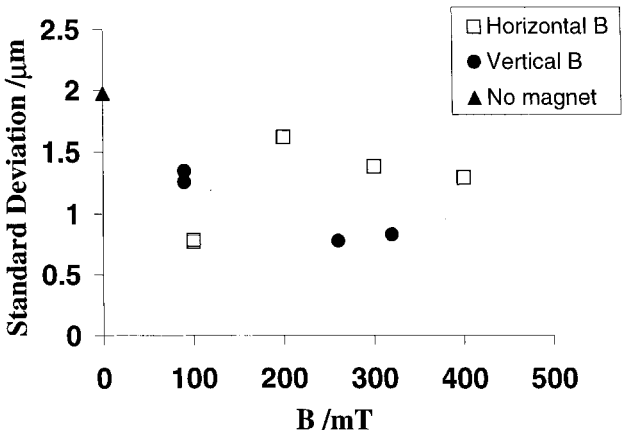

Fig. 7. Summary of the magnetic field effect on the standard deviation of the depth profile. Key: (□) horizontal *B*, (●) vertical *B* and (▲) no magnet.

within each sample. In the case of line profiles, the depth gradients would contribute significantly to the observed variance, while in the case of sections, the depth gradients would be minimized.

4. Detailed results of the statistical analysis

4.1. *Analysis based on the partitioned subsections*

In the analysis of an entire surface, both local roughness (i.e., point-to-point change in depth) and depth gradient influence the magnitude of the variance. The depth gradients essentially determine the range of measurements; their presence is due not only to current distribution on the sample surface, but also to the slight concavity/convexity of the samples and inexact determination of the geometric centre of samples. Since it is difficult (if possible at all) to determine the relative magnitude of these contributing factors, it is important to reduce the effect of depth gradients on the statistical analysis; hence the approach by partitioning. The results are assembled in Figures 8 and 9, showing the effect of magnetic field configuration. The positive/negative trends in standard deviation with respect to the absence of a magnetic field may also arise from the variation of local roughness with position within the sample, the existence of such variations is, indeed, signalled by Figure 6.

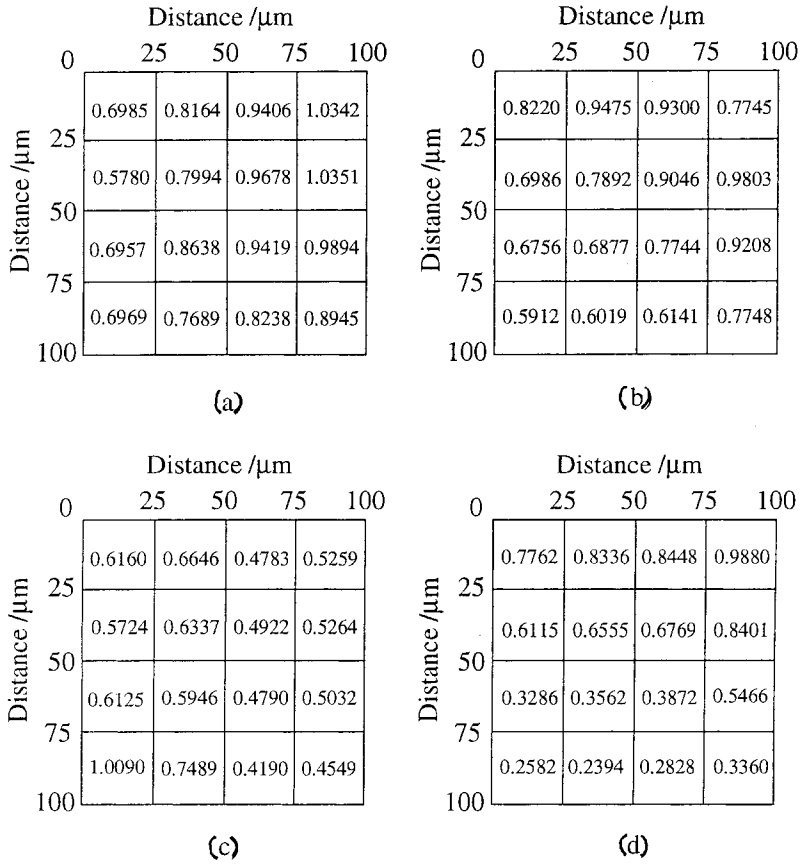

Fig. 8. Standard deviations of the depth profile in the partitioned surface areas exposed to a vertical magnetic field at flux densities (*B*) of: (a) 0, (b) 90, (c) 260 and (d) 320 mT.

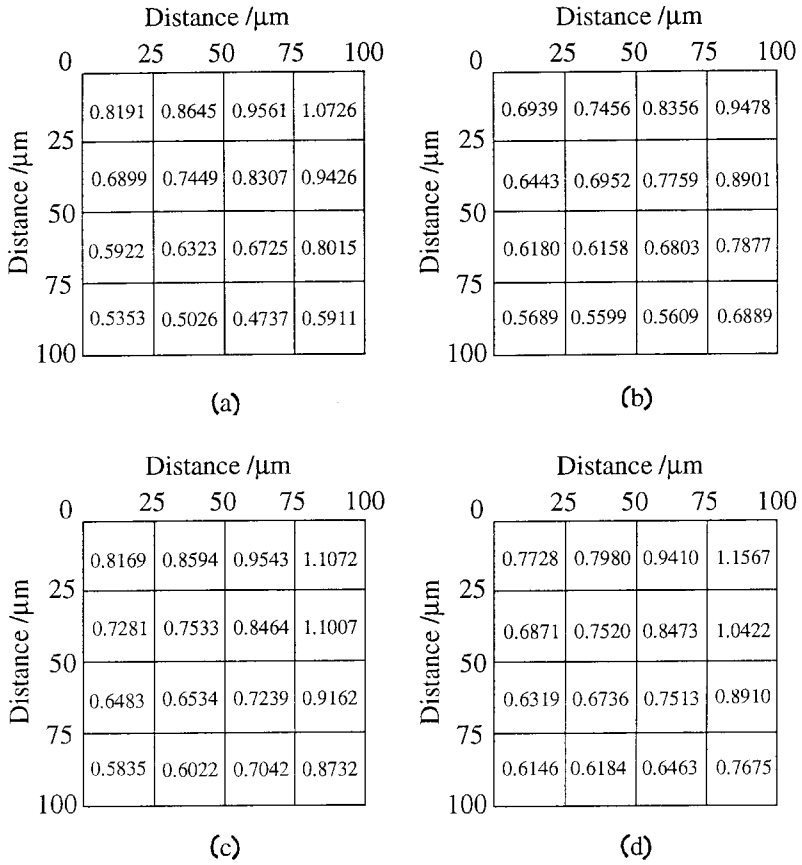

Fig. 9. Standard deviations of the depth profile in the partitioned surface areas exposed to a horizontal magnetic field at flux densities (B) of: (a) 100, (b) 200, (c) 300 and (d) 400 mT.

The magnetic field effect on the common variance is illustrated in Table 3. With the exception of the 100 and 200 mT horizontal flux densities, the results related to sample partitioning agree favourably with results related to the overall surface, in terms of the relative order of roughness. However, in contrast to the overall analysis (see Fig. 7), the lowest standard deviation is indicated in the case of the vertical magnetic field of 260 mT flux density. While this disagreement is not understood at present, it is possible that a low depth range, indicative of relatively small depth gradients within a sample, masks local roughness and makes the impression of better surface uniformity of a segment due to a small range of depths about the mean. Conversely, standard deviations calculated for samples possessing a larger depth range have a stronger contribution from existing depth gradients.

Table 3. Results of Bartlett's test of variance homogeneity for section variances within each sample

Orientation	B/mT	CVAR/μm^2	Chi-square
–	0	0.733 86	12 880.2
H	100	0.565 65	28 118.9
H	200	0.512 34	13 114.3
H	300	0.658 85	17 147.0
H	400	0.632 403	17 058.0
V	90	0.624 46	13 432.7
V	260	0.359 24	26 816.7
V	320	0.372 393	99 117.4

Common variance in sample (partitioned subsections)
CVAR $= [\Sigma_i s_i^2]/k; \quad i = 1, \ldots, k$

As shown in Tables 3 and 4, Bartlett's test rejects the null hypothesis of equal variances; this finding provides strong statistical support for the inference drawn by inspection of Figure 6. It is worth noting that the lowest variance related to the 100 mT strong horizontal field indicates the lowest depth gradient, as expected. The large magnitude of the test chi-square statistics for variances within each sample in Table 3 is primarily caused by the large sample size (16 384) used for each section. For samples of this magnitude, the variances would need to be numerically almost identical to be statistically equal. Comparison of the chi-square statistics and the critical chi-square value demonstrates that

Table 4. Results of Bartlett's test for homogeneity of variances about the section means

Field orientation	B/mT	VARSECM
–	0	3.3679
H	100	0.038 04
H	200	2.2620
H	300	1.0089
H	400	1.1038
V	90	1.2694
V	260	0.5028
V	320	0.3482

Legend: VARSECM = variance around the section mean
Test chi-square statistic = 63.676; Critical chi-square value = 14.1 ($\alpha = 0.05$) and 18.5 ($\alpha = 0.01$) with 7 degrees of freedom

deposit roughness depends strongly on the relative position within the sample.

4.2. *Analysis based on line segments*

The results of the test of homogeneity of variances are shown in Tables 5 and 6. The variance around the line means decreases monotonically (in fact, linearly with $r^2 = 0.95$) with increasing horizontal magnetic field strength. The variance decreases significantly in both field configurations with respect to the absence of a magnetic field, and the test chi-square statistic indicates that the magnetic field effect on surface roughness is statistically significant at any level of confidence. The common variance in sample obtained in testing variances of lines within samples also decreases linearly with magnetic field strength ($r^2 = 0.95$ and 0.93 in horizontal and vertical fields, respectively), and the magnetic field effect is clearly discernible due to the scatter of the chi-square values.

Table 5. Results of Bartlett's test for homogeneity of variances around line means

Field orientation	B/mT	VARLM/μm^2
–	0	2.6638
H	200	1.8662
H	300	0.9991
H	400	0.9055
V	90	0.9920
V	260	0.1102
V	320	0.3412

Legend: VARLM = variance around a line mean
Test chi-square = 25.06; the critical chi-square values are 12.6 ($\alpha = 0.05$) and 16.8 ($\alpha = 0.01$) with six degrees of freedom

Table 6. Results of Bartlett's test for homogeneity of variances of lines within samples

Orientation	B/mT	CVAR/μm^2	Chi-square
–	0	2.2096	195.3
H	200	1.4983	323.0
H	300	1.4773	660.6
H	400	1.1423	106.2
V	90	1.0921	133.6
V	260	0.5727	81.0
V	320	0.5795	574.7

CVAR is defined in Table 3
Critical values of chi-square as in Table 5

5. Concluding remarks

This paper demonstrates the utility of a combined employment of CSLBM and statistical variance analysis related to deposit roughness distribution in the study of cathode deposit quality. One attractive feature of the approach lies in the free choice of surface sectioning, in as much as the number of sections used in this study was arbitrarily set to sixteen in order to limit the size of computational requirements. Similar considerations apply to the number of line segments chosen.

External field effects on surface characteristics can be studied by various means; the only claim made here is that the approach described in the paper is one viable alternative.

Acknowledgement

This work was supported by the Natural Sciences and Engineering Research Council of Canada (NSERC). Dr S. Damaskinos of the Department of Physics provided valuable guidance in the use of the CSLB microscope in that department. Dr T. Duever in the Department of Chemical Engineering provided assistance in the statistical analysis.

Appendix: Summary of Bartlett's test for the homogeneity of variances

There are n_j samples taken from $j = 1, \ldots, k$ treatment populations. The null hypothesis is made that the variance due to experimental error within each of the populations is homogeneous. Textbooks on statistics usually present one of two variants of Bartlett's test, summarized below.

In the first variant (e.g. [17]) a chi-square test statistic is computed by the formula

$$\chi^2 = \left[\Sigma f_j \ln(MS_e) - \Sigma_j (f_j \ln(s_j^2))\right] \Big/ C \qquad (1)$$

where s_j^2 are the sample variances, $f_j = n_j - 1$,

$$MS_e = \left[\Sigma_j x_j^2 - (\Sigma_j x_j)^2/n\right] \Big/ \Sigma f_j \qquad (2)$$

$$C = 1 + \left[\Sigma_j(1/f_j) - 1/\Sigma_j f_j\right] \Big/ 3(k-1) \tag{3}$$

and x_j are the experimental observations.

If the chi-square value computed via Equation 1 is higher than the critical chi-square value with $k-1$ degree of freedom at a level of significance α, the null hypothesis is rejected at α. While the sample sizes may be different, the smallest size should not be less than three, and most sample sizes should be larger than five.

In the second variant (e.g. [18]) a pooled variance estimate is first computed as

$$s_p^2 = \Sigma_j(n_j - 1)s_j^2/(N-k); \quad N = \Sigma_j n_j \tag{4}$$

and the Bartlett test statistic is computed as

$$b = \left[\prod\nolimits_j (s_j^{u_j})\right]^{1/(N-k)} \Big/ s_p^2; \quad u_j = 2n_j - 2 \tag{5}$$

as a value of the random variable B possessing the Bartlett distribution. Critical values of the latter are tabulated (e.g. [18]; Table A. 10, pp.712–3) such that if b computed via Equation 5 is *smaller* than the critical value at a certain level of significance α, the null hypothesis is *rejected*. If the sample sizes are unequal, the critical b-value is computed as

$$b_k(\alpha; n_1, n_2, \ldots, n_k) = [\Sigma_j n_j b_j(\alpha; n_j)]/N \tag{6}$$

by 'pooling' the individual-size critical values computed via Equation 5.

The analysis shown in the main body of the paper employs a higher-dimensional computer-oriented version of the first variant. Simpler variance-homogeneity tests, for example, the Cochran and the Hartley test [17] require fewer calculations, but the sample sizes must be equal and the tests are more sensitive to deviations of the populations and the tests are more sensitive to deviations of the populations from normality.

For the sake of illustration, consider observations in the three treatment categories shown in the Table 7.

Following the first test-variant, $C = 1.1167$ and $MS_e = 2.0202$, yielding the test chi-square statistic of 0.549. Since the degree of freedom is 2, comparison with the critical chi-square values of 5.99 ($\alpha = 0,05$) and 9.21 ($\alpha = 0.01$) indicates that the null hypothesis (of equal population variances) cannot be rejected.

Table 7.

	4.7	5.0	8.0
	7.3	0.9	5.9
	5.9	3.2	8.1
	6.2	5.2	7.7
		3.6	4.8
		4.0	
n_j	4	6	5
s_j^2	1.143	2.423	2.175

Table 8.

	$\alpha = 0.05$	$\alpha = 0.01$
$b_3(\alpha, 4)$	0.4699	0.3165
$b_3(\alpha, 5)$	0.5762	0.4304
$b_3(\alpha, 6)$	0.6483	0.5149

In the second variant the pooled variance estimate is $s_p^2 = 2.0202$ and the test Bartlett-statistic is computed as $b = 0.9587$. Using the critical b-values shown in Table 8, the pooled critical values of b_3 (0.05; 4,5,6) = 0.5707 and b_3 (0.01; 4,5,6) = 0.4338 are obtained. It follows that the null hypothesis cannot be rejected.

References

1. A.M. El-Sherik and U. Erb, 'Production of nanocrystalline metals', *US Patent 07/983 205* (1992).
2. R.T.C. Choo, J.M. Toguri, A.M. El-Sherik and U. Erb, *J. Appl. Electrochem.* **25** (1995) 384.
3. O. Wassef and T.Z. Fahidy, *Electrochim. Acta* **21** (1976) 727.
4. O. Devos, A. Olivier, J.P. Chopart and O. Aaboubi, 'Magnetic field effects on nickel electrodeposition', Abstract 462, Joint International Meeting of the Electrochemical Society and the International Society of Electrochemistry, Paris, France **97-2** (1997), p. 561.
5. J.C. Shannon, 'Effect of magnetic field orientation on the electrodeposition of nickel', Project Report, University of Waterloo (1997).
6. J.C. Shannon, Z.H. Gu and T.Z. Fahidy, *J. Electrochem. Soc.* **144** (1997) L314.
7. A.E. Dixon, S. Damaskinos and M.R. Atkinson, *Nature* **351** (1991) 551.
8. Z.H. Gu, T.Z. Fahidy, S. Damaskinos and A.E. Dixon, *J. Electrochem. Soc.* **141** (1994) L153.
9. X. Ling, Z.H. Gu and T.Z. Fahidy, *Electrochim. Acta* **40** (1995) 1789.
10. Z.H. Gu, S.J. Xia and T.Z. Fahidy, *ibid.* **41** (1996) 2837.
11. D.S. Chung and R.C. Alkire, *J. Electrochem. Soc.* **144** (1997) 1529.
12. R.C. Alkire, 'Electrodeposition and dissolution of copper', Abstract 424, Joint International Meeting of the Electrochemical Society and the International Society of Electrochemistry, Paris, France **97-2** (1997), p. 517.
13. J. Feder, 'Fractals', (Plenum Press, New York, (1989), Chapters 8 and 9.
14. Z.H. Gu, J. Chen, A. Olivier and T.Z. Fahidy, *J. Electrochem. Soc.* **140** (1993) 408.
15. Z.H. Gu, J. Chen, T.Z. Fahidy and A. Olivier, *J. Electroanal. Chem.* **367** (1994) 7.
16. Z.H. Gu, S.J. Xia and T.Z. Fahidy, *Electrochim. Acta* **41** (1996) 2837.
17. B.J. Winer, 'Statistical Principles in Experimental Design', 2nd edn., Section 3.11, McGraw Hill, New York (1971).
18. R.E. Walpole and R.H. Myers, 'Probability and Statistics for Engineers and Scientists', 4th edn. Section 11.4, Macmillan, New York (1989).